Philosophical Magazine

ISSN: 1478-6435 (Print) 1478-6443 (Online) Journal homepage: http://www.tandfonline.com/loi/tphm20

On the effect of hydrogen on the elastic moduli and acoustic loss behaviour of Ti-6Al-4V

S. L. Driver, N. G. Jones, H. J. Stone, D. Rugg & M. A. Carpenter

To cite this article: S. L. Driver, N. G. Jones, H. J. Stone, D. Rugg & M. A. Carpenter (2016): On the effect of hydrogen on the elastic moduli and acoustic loss behaviour of Ti-6Al-4V, Philosophical Magazine, DOI: 10.1080/14786435.2016.1198054

To link to this article: http://dx.doi.org/10.1080/14786435.2016.1198054

Published online: 27 Jun 2016.

PHILOSOPHICAL MAGAZINE, 2016
http://dx.doi.org/10.1080/14786435.2016.1198054

Taylor & Francis
Taylor & Francis Group

OPEN ACCESS

On the effect of hydrogen on the elastic moduli and acoustic loss behaviour of Ti-6Al-4V

S. L. Driver[a,b], N. G. Jones[b], H. J. Stone[b], D. Rugg[c] and M. A. Carpenter[a]

[a]Department of Earth Sciences, University of Cambridge, Cambridge, UK; [b]Department of Materials Science and Metallurgy, University of Cambridge, Cambridge, UK; [c]Rolls-Royce plc., Derby, UK

ABSTRACT

The elastic moduli and acoustic loss behaviour of Ti-6Al-4V (wt.%) in the temperature range 5–298 K have been studied using Resonant Ultrasound Spectroscopy. A peak in the acoustic dissipation was observed at 160 K within the frequency range 250–1000 kHz. Analysis of the data acquired in this study, coupled with complementary data from the literature, showed that this was consistent with a Snoek-like relaxation process with an associated activation energy of 23 ± 3 kJ mol^{-1}. However, the loss peak was broader than would be expected for a Snoek-like relaxation, and the underlying process was shown to have a spread of relaxation times. It is suggested that this effect arises as a result of variations in the strain experienced by the β phase due to different local microstructural constraint by the bounding secondary α phase.

ARTICLE HISTORY
Received 21 January 2016
Accepted 31 May 2016

KEYWORDS
Titanium alloys; resonant ultrasound spectroscopy; microstructure; mobility; hydrogen in metals; internal friction

1. Introduction

Ti-6Al-4V (wt%) (Ti-6-4) is the most widely used titanium alloy, finding extensive applications in the aerospace industry. The microstructure is dominated by the hcp α phase, accompanied by a smaller volume fraction of the bcc β phase. As with other titanium alloys, aluminium preferentially partitions to the α phase, whilst vanadium stabilises the β phase. In addition, low concentrations of interstitial elements are also present, which can influence the phase equilibria and properties of the alloy [1]. Among such interstitials, oxygen is known to be a potent α phase stabiliser and provides significant strengthening [2]. In contrast, hydrogen is a β stabilising element and generally has a detrimental effect on the mechanical properties. Concentrations of ~130 wppm hydrogen have been reported to result in large reductions (~50%) in fracture toughness [3], whilst the propensity to suffer sustained load cracking and the associated crack growth rates also increase with elevated hydrogen contents [4]. Low levels of hydrogen in titanium alloys have also been implicated in poor cold dwell fatigue resistance [5,6]. The role of hydrogen in stress corrosion cracking is also highly significant, as local corrosion-induced hydrogen enrichment and migration to areas of high tensile stress facilitates crack extension [7].

CONTACT S. L. Driver sld64@cam.ac.uk

To avoid such issues, significant efforts are made to keep hydrogen levels low during manufacture, including the preferential use of electric rather than gas heat treatment furnaces, and the utilisation of hot vacuum degas operations. Whilst such methods allow hydrogen levels to be controlled and reduced, hydrogen uptake in service cannot always be avoided. Therefore, understanding the relative solubility and mobility of hydrogen in dual-phase titanium alloys is of considerable importance for industrial applications.

An early study characterising the internal friction of Ti-6-4 over a wide range of temperatures reported an acoustic loss peak at cryogenic temperatures [8]. However, the origin of this peak was not conclusively established. In later studies, it was shown that the height of the peak was affected by both hydrogen concentration and the dislocation density of the material, with the former dominating [9,10]. It was suggested that the acoustic loss resulted from the stress-induced movement of hydrogen interstitials in the β phase, known as the Snoek relaxation [9–11]. This conclusion was further supported by the disappearance of the acoustic loss peak when Ti–6–4 was tested after quenching from the β phase field, such that the microstructure was entirely α' martensite, with no retained β [9].

However, detailed analysis of the shape of this acoustic loss peak has shown that it is too broad to be described by a single relaxation process [8]. To date, no conclusive evidence has been reported that can satisfactorily explain this observation, indicating that further studies are required to understand the mobility and stress-induced movement of hydrogen in titanium alloys. Therefore, to gain further insight into the governing processes, resonant ultrasound spectroscopy (RUS) has been used to study the acoustic loss peak associated with hydrogen movement in Ti-6-4 over a range of frequencies in the kHz to MHz range and at temperatures between 5 and 298 K.

2. Experimental details

2.1. Sample

Ti-6-4 plate, which had been cross rolled in the $(\alpha + \beta)$ phase field followed by annealing at 700 °C for 2 h, was supplied by Rolls-Royce plc. The nominal composition of this material was 6.5 Al, 4.0 V, 0.18 Fe wt.%. The concentration of interstitial species in the material was measured by TIMET UK. A rectangular parallelepiped with dimensions of $3.03 \times 4.03 \times 5.02\,\text{mm}^3$ and a mass of 0.267 g (giving a calculated density of $4.36\,\text{g/cm}^3$) was machined by Brite Precision Ltd. The faces were polished to remove the surface layer affected by machining.

2.2. Resonant ultrasound spectroscopy

The principles and protocols of RUS have been outlined by Migliori & Sarrao [12] and the reader is referred to the work of McKnight et al. [13] for a detailed description of the particular RUS instrument used in the present study.

RUS measurements were performed in a helium flow cryostat with the sample held directly between the driving and receiving piezoelectric transducers. Room temperature spectra were acquired first, in the frequency range 100–1000 kHz, with 50 000 data points in each spectrum. Data obtained below room temperature were collected during isothermal holds between 100 and 1200 kHz, with 130 000 data points in each spectrum. On cooling, RUS spectra were acquired at 5 K intervals between 295 and 200 K; 10 K intervals between

200 and 190 K; 30 K intervals between 190 and 10 K; and 5 K intervals between 10 and 5 K. On heating, RUS spectra were acquired at 5 K intervals between 5 and 295 K. A period of 20 minutes was allowed for thermal equilibration at each temperature prior to data collection.

The RUS spectra were analysed using the software package Wavemetrics IGOR PRO. Each resonance peak was fitted with an asymmetric Lorentzian function to accurately determine the peak frequency, f, and the full width at half of the maximum height, Δf. In RUS, f^2 scales with the elastic constants of the material, with the main contribution coming from the shear modulus in the case of a polycrystalline sample. In order to determine average bulk and shear moduli, the frequencies of up to 58 resonance peaks were obtained from each spectrum. For each resonance, the inverse mechanical quality factor, Q^{-1}, which may be taken as $Q^{-1} = \Delta f / f$, provided a measure of the acoustic dissipation.

2.3. Elastic constant calculation

The rectangular parallelepiped resonance (RPR) code was used to convert the experimental resonant frequencies into elastic moduli. This code is available online [14], and explained in more detail elsewhere [15]. It operates by estimating the elastic constants for the sample and using these to calculate the expected resonant frequencies, which are then compared to those obtained through experiment. The elastic constant estimates are then modified iteratively until the calculated and experimental frequencies match.

For the measurements made at room temperature, 58 resonant frequencies were included in the code, whilst 30 to 41 resonant frequencies were used for the low-temperature data, depending upon the quality of the data acquired at each temperature. The 'goodness-of-fit' between the observed and calculated resonances was reported as an RMS error, giving a measure of the reliability of the result.

Hill averages of the Young's and shear moduli for the sample were calculated from the fitted orthotropic elastic constants using the ElAM program [17].

2.4. Microstructural characterisation

A sample of Ti-6-4 was sectioned and mounted in conductive bakelite before being ground and polished using a protocol terminating in a 0.25 μm colloidal silica suspension. Backscattered electron imaging of the microstructure was performed using an FEI Nova NanoSEM 450 operating at 15 kV and a working distance of 5 mm.

3. Results

3.1. Material condition

The concentrations of interstitial species determined by LECO analysis were 0.007 wt.% C, 1973 ppm O, 46 ppm N, 23.68 ppm H. These were all within the industry standard specification for AMS 4911.

Backscattered electron micrographs of the as-received material at varying magnifications are shown in Figure 1. At the lowest magnification, Figure 1(a), the microstructure can be seen to consist of globular primary α phase, ~10–40 μm in diameter, interspersed with transformed β regions containing high aspect ratio α plates, separated by layers of

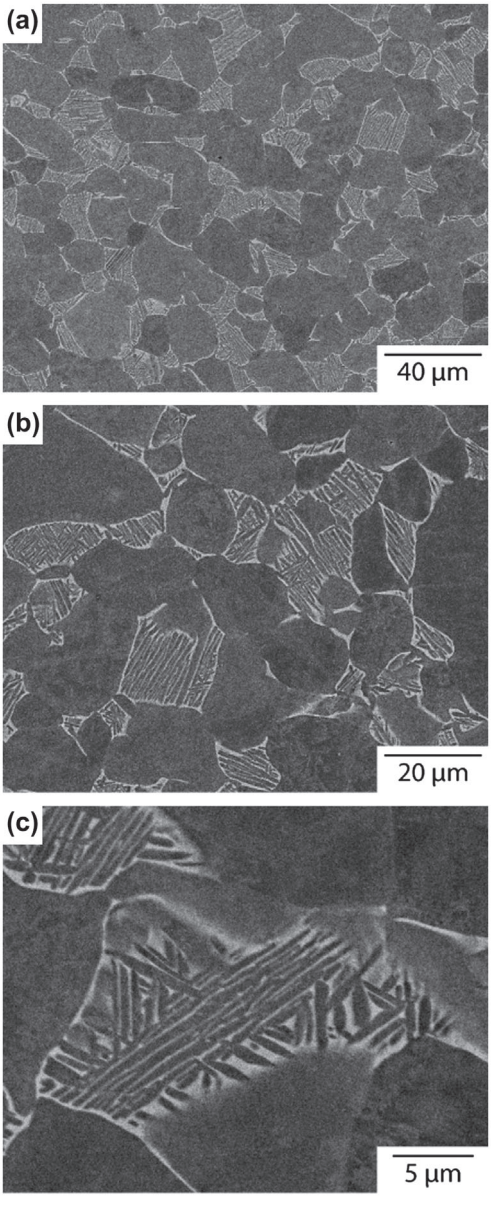

Figure 1. Backscattered electron images of the microstructure of the as-received material.

retained β. At higher magnification, Figure 1(b), it can be seen that individual regions of transformed β had different configurations of α variants, some being dominated by a single variant (colony-like) whilst others showed a number of variants, exhibiting a more basket-weave-like structure. Closer inspection of a region of transformed β, Figure 1(c), showed that there was significant variation in the thickness of the retained β layers between the α plates. For example, in the central colony the α laths were interspersed by very fine retained β layers, ~300 nm wide, whilst in the surrounding basket-weave regions, the retained β was almost an order of magnitude thicker.

Table 1. Elastic tensor components at room temperature determined assuming different elastic tensor symmetries.

	Elastic stiffness / GPa									
	c_{11}	c_{22}	c_{33}	c_{23}	c_{13}	c_{12}	c_{44}	c_{55}	c_{66}	RMS error
isotropic	154	–	–	62	–	–	46	–	–	1.1%
axisymmetric	168	–	173	77	–	83	46	–	43	0.32%
orthotropic	172	171	175	81	79	87	46	47	42	0.19%

Table 2. Room temperature elastic moduli of Ti-6-4 from RUS experiments, alongside values published in the literature.

Source	K / GPa	E / GPa	G / GPa
RUS study	113	119	45
Ref. [19]	105	111	42.0
Ref. [20]	75 – 135	106 – 113.5	40 – 45
Ref. [21]	113	110	
Ref. [22]		107 – 121	42.1
Ref. [23]		103	
Ref. [24]		108 – 117	
Ref. [25]		113	
Ref. [26]		118	
Ref. [27]		110 – 114	
Ref. [28]		116	
Ref. [29]		108	
Ref. [30]		115	
Ref. [31]		117	
Ref. [32]		102	
Ref. [33]		122	

3.2. Room temperature elastic properties

Table 1 shows the components of the full elastic tensor obtained at room temperature. The material studied had been cross-rolled. As a consequence, a significant rolling texture would be expected [16], leading to elastic anisotropy with the transverse and longitudinal directions having similar elastic constants. Therefore, the macroscopic elastic tensor should either possess an axisymmetric or orthotropic average symmetry.

The room temperature resonant frequencies were initially fitted using isotropic elastic symmetry, with two independent constants, and gave a high RMS error of 1.1%. Fitting the room temperature resonant frequencies assuming an axisymmetric elastic symmetry, with five independent elastic constants, gave an RMS error of 0.32%. In comparison, an RMS error of less than 0.2% was obtained assuming orthotropic sample symmetry, with 9 independent elastic constants. Therefore, all subsequent analyses were performed assuming orthotropic symmetry.

Hill averages of the bulk modulus, K, Young's modulus, E, and shear modulus, G, were obtained from the orthotropic elastic constants using the ElAM code, Table 2. This approach, rather than direct fitting of the RUS data assuming isotropic symmetry, was adopted as the values obtained were in better agreement with previously published values (see Table 2).

The apparent Young's modulus of commercially available Ti-6-4 products may vary between 107 and 132 GPa, depending upon the loading direction and the texture of the

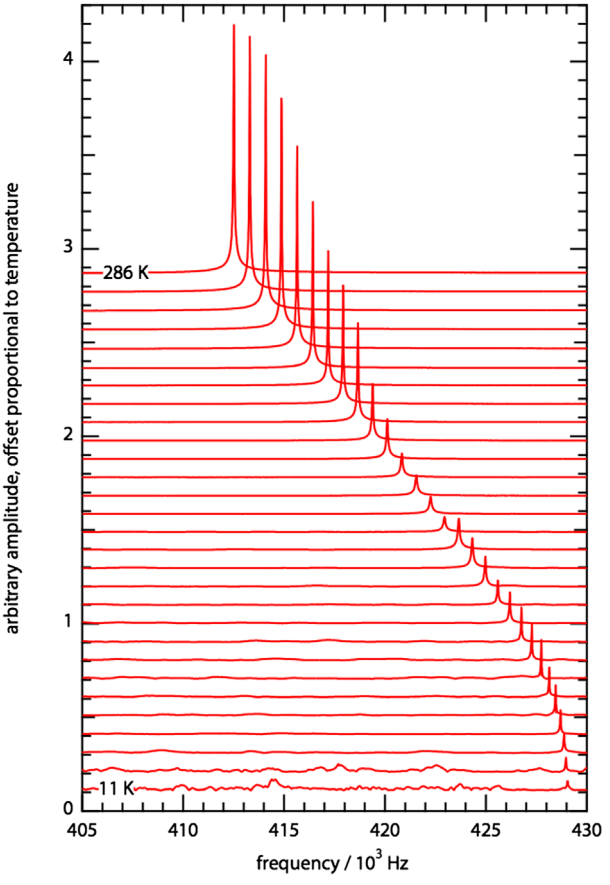

Figure 2. (colour online) Section of the RUS spectra collected around a single resonance peak showing the change of the resonance frequency with temperature between 11 and 292 K. Each spectrum is offset on the *y*-axis in proportion to the temperature at which it was collected.

material [18] (see Table 2). The values of 125, 117 and 114 GPa obtained from RUS data at room temperature for each of the three principal directions of the sample compare favourably with this range.

3.3. Low temperature

A section of the RUS spectra around one resonance peak, collected between 405 and 430 kHz and at temperatures between 11 and 292 K, is shown in Figure 2. The amplitude is shown on the vertical axis, with each spectrum also offset by an amount proportional to the temperature at which it was collected.

The resonance frequency of the peak increased approximately linearly as the temperature was lowered until ~100 K, below which it asymptotically approached an almost constant value. The peak was sharp at room temperature, and maintained a constant width with decreasing temperature until ~220 K. The width then increased, reaching a maximum at ~160 K, before becoming sharper again.

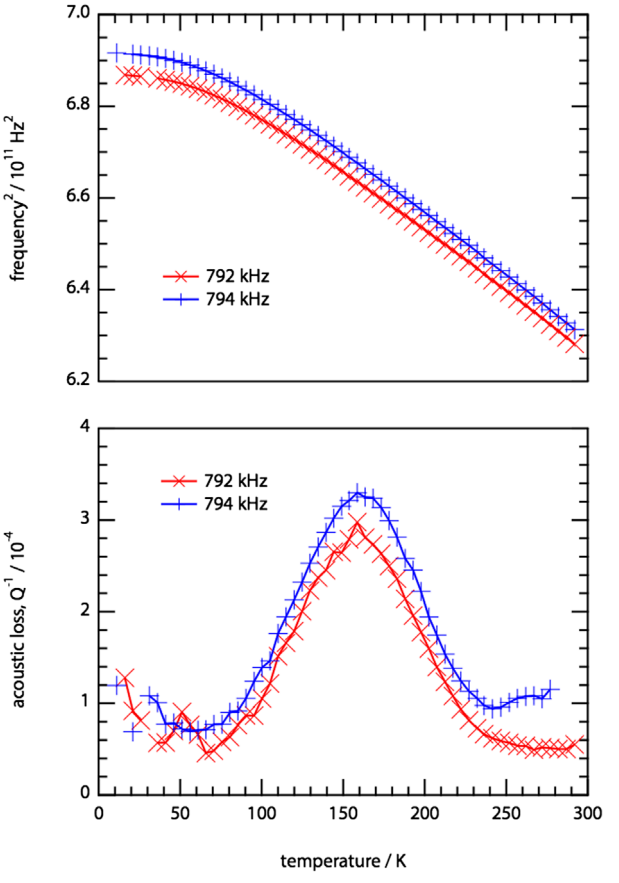

Figure 3. (colour online) The effect of temperature on f^2 (proportional to the effective modulus) and Q^{-1} (measure of acoustic dissipation) for two resonances.

The behaviour of the squared resonance frequency, f^2, and the inverse quality factor, Q^{-1}, of two resonances are shown in Figure 3. The labels used in the legend indicate the frequency of the resonance at room temperature. A nearly symmetrical Debye loss peak was observed in all resonances between 60 and 230 K, with a maximum at approximately 160 K. The behaviour of f^2 was smooth throughout, indicating no obvious deviation in the elastic properties at the temperature where the acoustic loss maximum was observed.

4. Analysis and discussion

4.1. Elastic properties

The values of the average elastic moduli between 10 and 298 K obtained from the RPR and ElAM codes are shown in Figure 4. A < 10% variation in the average shear and Young's moduli and a < 5% variation in the bulk modulus were observed over the temperature range studied. The change in the average Young's modulus with temperature is consistent with previously published results [19,34,35].

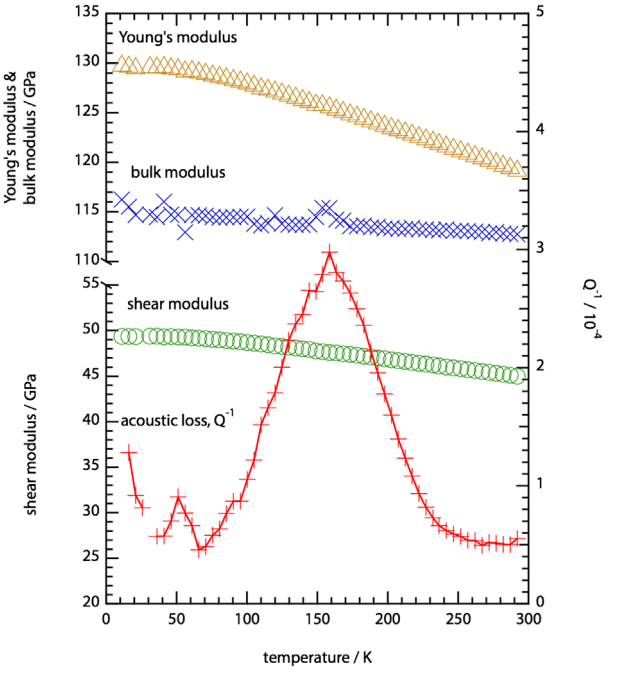

Figure 4. (colour online) Average Young's (gold triangle markers), shear (green circle markers) and bulk (blue cross markers) moduli as a function of temperature between 10 and 298 K. The acoustic dissipation peak is also shown for reference (red 'plus' markers connected by a line). The experimental uncertainties in all of the measured values are smaller than the markers used.

As seen in Figure 2, the change of resonant frequency with temperature was smooth and, therefore, the evolution of the elastic constants would also be expected to be smooth [36]. This was apparent for the Young's and shear moduli, but not for the bulk modulus, which exhibited significant scatter in certain temperature ranges. As the resonance modes of a polycrystalline sample excited during RUS are mainly of shear character, their sensitivity to the bulk modulus is weaker. A large number of resonant peaks were used in the determination of the elastic properties in an effort to reduce uncertainty in the determination of the bulk modulus [37]. However, increased scatter was still observed for certain temperature ranges, which was associated with inferior peak sampling. This arose as a result of fewer peaks being resolvable, due to either increased acoustic loss, or at very low temperatures where the signal from the transducer was weak.

The temperature dependence of the acoustic loss, Q^{-1}, has also been plotted in Figure 4. It is expected that any Debye relaxation process would lead to a marked change in the modulus at the temperature associated with the maximum acoustic loss [38]. However, no evidence of such a change in the elastic properties can be discerned from the modulus data around the temperature at which the maximum acoustic loss occurs, beyond the range of experimental uncertainty. As such, it can be concluded that the process governing the acoustic loss involves only small strains within the material.

Table 3. Activation energy and frequency factor obtained for the acoustic loss process investigated in this study. Literature values are also included for comparison.

Source	Hydrogen content	Activation energy, E_{act} kJ/mol	Activation energy, E_{act} eV	Frequency factor, ν_0 s^{-1}
Ref. [8]		21.6	0.224	5.85×10^{10}
Ref. [9]	0.612 at.%	27.0	0.280	7.06×10^{14}
Ref. [10]	116 ppm	20.3 ± 1.9	0.21 ± 0.02	10^{15}
Ref. [11]	50 ppm	23 ± 2.1	0.24 ± 0.02	4.0×10^{14}
RUS study + Ref. [8–11,40]		23 ± 3	0.24 ± 0.03	3.6×10^{12}

4.2. Acoustic losses

The relationship between acoustic loss, Q^{-1}, and frequency, f, of a Debye relaxation process is given in Equation (1):

$$Q^{-1} = \Delta \frac{\omega\tau}{1 + \omega^2\tau^2} \tag{1}$$

where $\omega = 2\pi f$ is the angular frequency, τ is the relaxation time and Δ is a constant. τ^* is used to denote the relaxation time at the maximum value of the acoustic loss, Q_m^{-1}, for a particular frequency and is given by $\omega\tau^* = 1$.

If the process giving rise to an acoustic loss peak is thermally activated, then it will have an associated activation energy, E_{act}. The relaxation time of the loss process, τ, as a function of temperature is given by the Arrhenius equation [38,39]:

$$\tau = \frac{1}{\nu_0} \exp\left(\frac{E_{act} + PV_{act}}{RT}\right) \tag{2}$$

where the frequency factor, ν_0, is a constant.

An Arrhenius plot of $\ln \tau^*$ against T^{-1}, obtained from the data acquired in this study, as well as values taken from the literature, is given in Figure 5. The inverse temperature at which the maximum acoustic loss occurred did not appear to change significantly with excitation frequency for any of the peaks observed using RUS. This suggests that the process is either athermal or has a very small activation energy, which does not give a measurable variation with temperature within the frequency range investigated in this study.

To examine how the temperature of the maximum acoustic loss varies over a much wider range of frequencies, data obtained from previous studies using a variety of alternative techniques [8–11,40] have been included in Figure 5. Collectively, these data indicate that the temperature of maximum acoustic loss does vary with frequency. A linear fit through all of the data including an average value from the results of this study yielded an activation energy of 23 ± 3 kJ mol^{-1}. This activation energy is in good agreement with the values reported previously for relaxation processes in Ti-6-4, as shown in Table 3. Critically, this value is also similar to the activation energy reported for the diffusion of hydrogen in the β phase of pure titanium [41,42] and Ti–13V–11Cr–3Al [43]. Therefore, the acoustic loss peak appears to be associated with a Snoek-like relaxation of hydrogen in the β phase of Ti-6-4, as suggested previously [9–11].

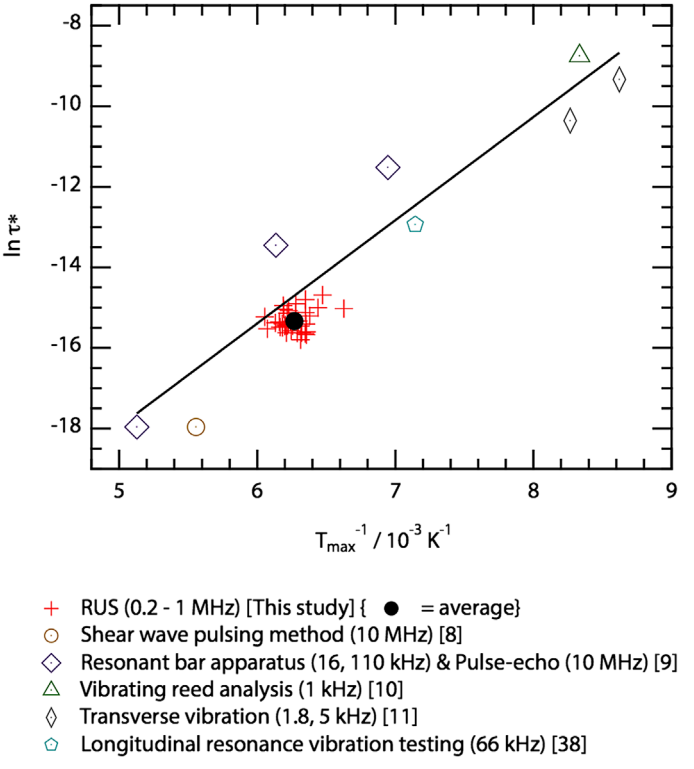

Figure 5. (colour online) Arrhenius plot showing ln τ^* against T^{-1}, including literature values [8–11,40].

The frequency factor, ν_0, obtained from the linear fit to the Arrhenius plot was calculated to be $3.6 \times 10^{12}\ s^{-1}$, which is lower than that reported previously, Table 3. This was also lower than the value of $\sim 10^{14}\ s^{-1}$ expected for Snoek-like behaviour [38]. However, it is not possible to entirely rule out the effect of dislocations, which have been attributed to relaxation processes with frequency factors in the range 10^{10}–$10^{12}\ s^{-1}$ [9,38].

Interstitial hydrogen may move between neighbouring octahedral or tetrahedral sites, and the relaxation times expected for the movement of atoms between interstices can be calculated using Equation 3 [38];

$$D = \frac{a^2}{z\tau} \tag{3}$$

where D is the diffusivity, a is the lattice parameter, and z is a constant related to the distance and direction of each atomic movement (36 for octahedral–octahedral and 72 for tetrahedral–tetrahedral). Using the diffusivity of hydrogen in β titanium, calculated from the equation given by Wasilewski and Kehl [42], and the lattice parameter for the β phase in Ti-6-4 reported by Malinov et al. [44], the relaxation time at 298 K for octahedral-octahedral movement, τ_{oct}, was calculated to be 1.1×10^{-9} s and for tetrahedral–tetrahedral movement, τ_{tet}, as 5.6×10^{-10} s. The relaxation time determined from the experimental values aggregated in the present study, τ_{av}, is 3.4×10^{-9} s. This is on the order of τ_{oct}

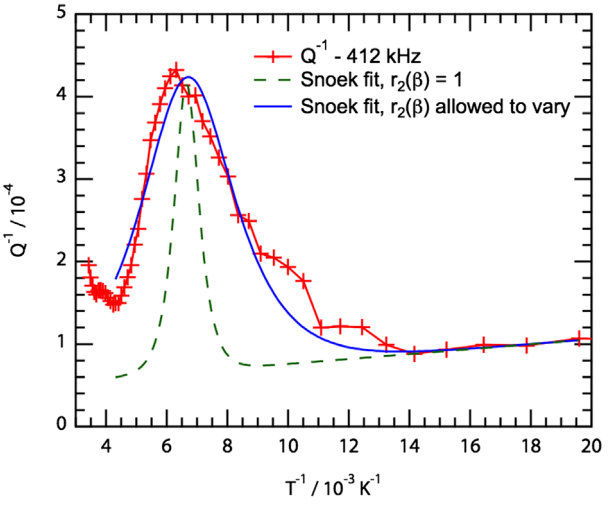

Figure 6. (colour online) Behaviour of Q^{-1} with inverse temperature for the resonance with frequency 412 kHz at 298 K. Two fits for Snoek-like behaviour, with E_{act} fixed at 23 kJ mol^{-1} are also shown. The result of the fit with the value of $r_2(\beta)$ fixed at 1 is shown with the dashed green line, whilst the solid blue line shows the result when $r_2(\beta)$ was allowed to vary.

estimated above and is therefore consistent with previous studies that have concluded that hydrogen occupies the octahedral interstitial sites in β titanium [45–47].

In addition to the position of the peak maximum, the form of the acoustic loss peak gives information about the nature of the associated process. For a Snoek relaxation, the temperature dependence of Q^{-1}, for a given frequency, is described by Equation 4 [48,49];

$$Q^{-1}(T) = Q_m^{-1}\left[\cosh\left\{\frac{E_{act}}{R\, r_2(\beta)}\left(\frac{1}{T}-\frac{1}{T_{max}}\right)\right\}\right]^{-1} \quad (4)$$

where Q_m^{-1} is the maximum value of Q^{-1} occurring at temperature T_{max} and E_{act} is the activation energy of the process. $r_2(\beta)$ is the relative width of the acoustic loss peak assuming a Gaussian distribution of relaxation times, compared to the width of a Debye peak, which has a single relaxation time [38].

Experimental values of Q^{-1} for a typical acoustic loss peak (412 kHz at 298 K) as a function of inverse temperature are shown in Figure 6. If these data corresponded to a classical Snoek relaxation process, then it should have a single activation energy and relaxation time. Under such circumstances, $r_2(\beta)$ will equal 1. Fitting the experimental data for Q^{-1} using Equation 4 with $r_2(\beta) = 1$ and $E_{act} = 23$ kJ mol^{-1}, shown by the dashed green line in Figure 6, did not adequately describe the data. As such, the assumption that the acoustic loss process has a single activation energy and a single relaxation time does not appear to be valid.

The broadness of the acoustic loss peak may result from the existence of relaxation processes with a range of activation energies, a spread of relaxation times, or both. It has been shown by Niblett [50] that a plot of acoustic loss peak width, ΔT^{-1}, as a function of the inverse temperature at which the peak occurs, $1/T_{max}$, can give an indication whether the activation energy and relaxation time have single values, or vary. If the resultant plot

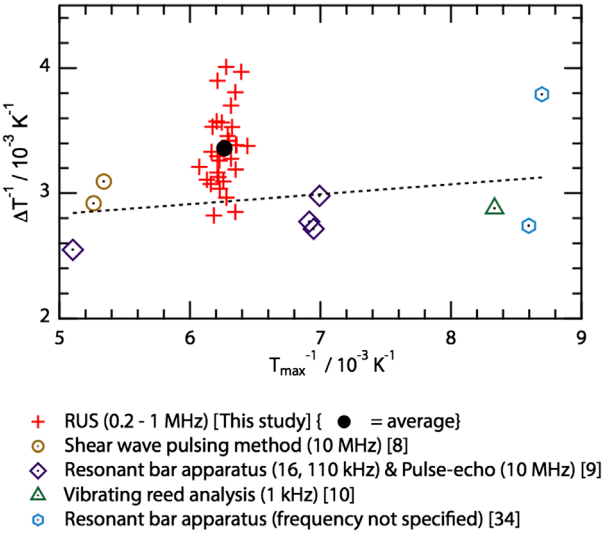

Figure 7. (colour online) A plot of ΔT^{-1} against $1/T_{max}$ following Niblett [50], including results from this study and the literature [8–10,34]. The results (except [34]) all lie on a line with zero gradient within error, suggesting that there is only one activation energy for the acoustic loss process.

has a positive gradient, the acoustic loss peak has a spread of activation energies, whereas a flat plot indicates a single activation energy with either a single relaxation time or a distribution of relaxation times.

Again, by combining data acquired in the present study, from 30 acoustic loss peaks, with data published in the literature [8–10,34], ΔT^{-1} was plotted as a function of $1/T_{max}$ over a frequency range of 1 kHz–10 MHz, Figure 7. A linear fit to all of the data has been included as a dashed line. The gradient of the fit is 0.08 ± 0.09, which suggests that the relaxation process leading to the acoustic loss has a single activation energy. As such, the breadth of the acoustic loss peak, shown in Figure 6, was believed to be due to the associated acoustic loss process having a range of relaxation times.

The data for Q^{-1}, shown in Figure 6, were refitted with Equation 4 whilst permitting $r_2(\beta)$ to vary, in line with the underlying process having a range of relaxation times. The resultant curve is shown by the solid blue line in the figure and provides a good description of the experimental observations. By fitting the acoustic loss peak observed in 11 different resonances in the same way, a value for $r_2(\beta)$ of 3.65 ± 0.06 was obtained, meaning that the observed peak is around 3.5 times wider than that expected for a Debye peak.

In order to calculate the expected relaxation strength, the Debye peak height must be measured. When $r_2(\beta)$ is greater than 1, the observed peak height is lower than that for a Debye peak. As the form of the anelastic loss is not expressible as a tabulated function, asymptotic expressions were used to calculate β [51], describing the width of the relaxation time distribution via:

$$r_2(\beta) = \frac{\Delta_2 x'(\beta)}{\Delta_2 x'(0)} \tag{5}$$

where

$$\Delta_2 x'(\beta) \sim 0.723\beta \tag{6}$$

and

$$\Delta_2 x'(0) = 1.144 \tag{7}$$

The relative peak height, $f_2(0, \beta)$, asymptotically approximates to;

$$f_2(0, \beta) \sim \frac{\sqrt{\pi}}{2\beta} \tag{8}$$

Values for β and $f_2(0, \beta)$ obtained from the experimental data were ~ 5.7 and ~ 0.16, respectively. The value of $f_2(0, \beta)$ obtained was subsequently used to calculate the relaxation strength, $\delta J/J_u$, which is the change in the elastic compliance, δJ, divided by the unrelaxed compliance, J_u, via Equation 9 [38];

$$Q_{\mathrm{m}}^{-1} = \frac{\delta J}{J_u} f_2(0, \beta) \tag{9}$$

A value of 2.2×10^{-3} was obtained for $\delta J/J_u$, which indicated that the change in the modulus due to the relaxation process was very small. This observation is consistent with the elastic modulus results shown in Figure 4, where no noticeable deviation occurred at the temperature of maximum acoustic loss. This also follows the expectation that the movement of hydrogen atoms between interstitial sites in the β phase, which constitutes a very small fraction of the microstructure, would only produce a slight change in elastic properties.

Using the value of β, obtained from fitting the acoustic loss peak, the distribution of relaxation times, Φ, was determined to be $-4 \times 10^{-9} + 0.105 \exp\{(z + 28.9)/\beta\}$, where $z = \ln(\tau/\tau_{\mathrm{av}})$. This wide spread in relaxation times indicates that there may be inhomogeneity in the octahedral interstices of the β phase. It has been reported previously that substitutional elements have an effect on the form of the Snoek peak (for example, in Fe–C–M alloys [52,53] and in Fe–Cr alloys [54]). It is therefore possible that V in the β phase may contribute to the increased width of the acoustic loss peak. Alternatively, it may arise as a result of inhomogenous strains across the microstructure. As may be seen in Figure 1, the microstructural constraint imposed on the β phase channels by the surrounding α phase varied significantly. As a result, the strain field present in each channel may be heterogeneous, due to microstresses arising from elastic, plastic and thermal anisotropy between the phases. In turn, these strain fields will affect the degree of distortion of the octahedral interstices. It is therefore possible that this leads to a spread of relaxation times of the interstitial hydrogen movement, though further study to confirm this hypothesis is required.

5. Conclusions

The elastic and acoustic loss behaviour of Ti-6-4 at temperatures between 5 & 298 K was studied using Resonant Ultrasound Spectroscopy. A wide acoustic loss peak was observed, centred at 160 K when measured between 250 & 1000 kHz. The temperature at which the acoustic loss peak occurred was observed to change with frequency between 1 kHz and 10 MHz, from which it was concluded that the underlying process was thermally activated. An activation energy of 23 ± 3 kJ mol^{-1} was obtained, which is close to the activation energy of diffusion of hydrogen in β titanium. The relaxation time and frequency factor

of the process are consistent with the peak being caused by a Snoek relaxation; the stress-induced movement of hydrogen interstitials between octahedral sites in the β phase.

Values of the isotropic (bulk, shear and Young's) elastic moduli were also obtained. No abrupt change in any of the moduli was seen at 160 K, contrary to what would be expected for a Debye relaxation. This was shown to be a result of the small value for the relaxation strength, and was consistent with the expectation that the movement of hydrogen interstitials between sites would not significantly affect the elastic properties.

The width of the acoustic loss peak was much wider than that expected for a Snoek relaxation process with a single value for the activation energy and relaxation time. Detailed analysis revealed that the process had a single value for the activation energy, and that the width was caused by a spread of relaxation times. The microstructure of the alloy contained a range of β-channel widths in and between the basket-weave and colony-like areas of the secondary α phase. Any differences in the strain experienced by the β channels as a result of local microstructural constraint would influence the octahedral interstices and could lead to the spread of relaxation times observed.

Note

The underlying data for this study can be found at https://www.repository.cam.ac.uk/handle/1810/256150.

Acknowledgements

The authors would like to acknowledge Dr M Thomas of TIMET UK for providing compositional analysis.

Disclosure statement

No potential conflict of interest was reported by the authors.

Funding

This work was supported by the EPSRC / Rolls-Royce Strategic Partnership [grant number EP/H022309/1], [grant number EP/H500375/1], [grant number EP/M005607/1]; and Natural Environment Research Council of Great Britain [grant number NE/B505738/1], [grant number NE/F017081/1].

ORCID

S. L. Driver http://orcid.org/0000-0003-2151-0221
N. G. Jones http://orcid.org/0000-0002-1851-2261
H. J. Stone http://orcid.org/0000-0002-9753-4441

References

[1] H. Conrad, Prog. Mater. Sci. 26 (1981), p. 123. Available at http://www.sciencedirect.com/science/article/pii/0079642581900013.

[2] Q. Yu, L. Qi, T. Tsuru, R. Traylor, D. Rugg, J.W. Morris, M. Asta, D.C. Chrzan, and A.M. Minor, Science 347 (2015), p. 635. Available at http://www.sciencemag.org/content/347/6222/635.full.
[3] J.D. Cotton, P.J. Hellenbrand, D.J. Bryan, T.D. Bayha, M. Leder, and I. Levin, *The effect of hydrogen on the fracture toughness of Ti-5Mo-5V-5Al-3Cr*, in TMS 2014 Supplemental Proceedings, John Wiley & Sons, Inc., Hoboken, NJ, USA, 2014, doi: 10.1002/9781118889879.ch10.
[4] R.R. Boyer and W.F. Spurr, Metall. Trans. A 9 (1978), p. 23. Available at http://link.springer.com/10.1007/BF02647166.
[5] W. Evans and M. Bache, Scr. Metall. Mater. 32 (1995), p. 1019. Available at http://www.sciencedirect.com/science/article/pii/0956716X95000687.
[6] A.L. Pilchak and J.C. Williams, Metall. Mater. Trans. A 42 (2010), p. 1000. Available at http://link.springer.com/10.1007/s11661-010-0507-9.
[7] T. Chapman, R. Chater, E. Saunders, A. Walker, T. Lindley, and D. Dye, Corros. Sci. 96 (2015), p. 87. Available at http://www.sciencedirect.com/science/article/pii/S0010938X15001407.
[8] W. Mason and J. Wehr, J. Phys. Chem. Solids 31 (1970), p. 1925. Available at http://www.sciencedirect.com/science/article/pii/0022369770901873.
[9] N. Guiles and K. Ono, *The effect of hydrogen on internal friction of several titanium alloys*, in *Effect of hydrogen on behavior of materials*, A. Thompson and I. Bernstein, eds.,Metall. Soc. AIME, New York, 1976, pp. 666–674.
[10] S. Amadori, E. Bonetti, L. Pasquini, P. Deodati, R. Donnini, R. Montanari, and C. Testani, Mater. Sci. Eng.: A 521–522 (2009), p. 340. Available at http://linkinghub.elsevier.com/retrieve/pii/S0921509309002615.
[11] J. Du, Journal de Physique Colloques C5(42) (1981), p. 775. Available at http://jphyscol.journaldephysique.org/articles/jphyscol/abs/1981/05/jphyscol198142C5120.html.
[12] A. Migliori and J. Sarrao, *Resonant Ultrasound Spectroscopy: Applications to Physics, Material Measurements and Nondestructive Evaluation*, Wiley, New York, 1997.
[13] R.E.A. McKnight, M.A. Carpenter, T.W. Darling, A. Buckley, and P.A. Taylor, Am. Mineral. 92 (2007), p. 1665. Available at http://ammin.geoscienceworld.org/cgi/doi/10.2138/am.2007.2568.
[14] http://www.magnet.fsu.edu/inhouseresearch/rus/index.html
[15] A. Migliori, J. Sarrao, W. Visscher, T. Bell, M. Lei, Z. Fisk, and R. Leisure, Physica B 183 (1993), p. 1. Available at http://www.sciencedirect.com/science/article/pii/092145269390048B.
[16] G. Lütjering, Mater. Sci. Eng.: A 243 (1998), p. 32. Available at http://www.sciencedirect.com/science/article/pii/S0921509397007788.
[17] A. Marmier, Z.A.D. Lethbridge, R.I. Walton, C.W. Smith, S.C. Parker, and K.E. Evans, Comput. Phys. Commun. 181 (2010), p. 2102. Available at http://linkinghub.elsevier.com/retrieve/pii/S0010465510003401.
[18] M. Bache and W. Evans, Mater. Sci. Eng.: A 319–321 (2001), p. 409. Available at http://www.sciencedirect.com/science/article/pii/S0921509300020347.
[19] E. Naimon, W. Weston, and H. Ledbetter, Cryogenics 14 (1974), p. 246. Available at http://linkinghub.elsevier.com/retrieve/pii/0011227574902239.
[20] Y.T. Lee, M. Peters, and G. Welsch, Metall. Trans. A 22 (1991), p. 709. Available at http://link.springer.com/article/10.1007/BF02670293.
[21] *Materials properties data book. Volume I. Introduction and light metals*, Report No: AGC-2275, Tech. Rep., Aerojet Nuclear Systems Co., U.S. Department of Energy, Sacramento, CA, 1970. Available at http://www.osti.gov/scitech/biblio/4240042.
[22] F.R. Schwartzberg, S.H. Osgood, R.D. Keys, and T.F. Kiefer, Martin Marietta Corporation, *Cryogenic materials data handbook*, AFML Rep No ML-TDR-64-280, Compiler: M. Knight, Air Force Materials Laboratory, 1970.
[23] S. Hanlein, W. Hinckley, and F. Stecher, *NOLTR Report 70–141: Comparison of Mechanical and Acoustic Properties for Selected Nonferrous, Ferrous, and Plastic Materials*, Tech. Rep, United States Naval Ordinance Laboratory, White Oak, MD, 1970.

[24] Z. Fan, Scr. Metall. Mater. 29 (1993), p. 1427. Available at http://www.sciencedirect.com/science/article/pii/0956716X9390331L.
[25] I. Sen and U. Ramamurty, Scr. Mater. 62 (2010), p. 37. Available at http://linkinghub.elsevier.com/retrieve/pii/S1359646209005934.
[26] A.K. Swarnakar, O. Biest, and B. Baufeld, J. Mater. Sci. 46 (2011), p. 3802. Available at http://link.springer.com/10.1007/s10853-011-5294-1.
[27] M. Niinomi, Mater. Sci. Eng.: A 243 (1998), p. 231. Available at http://linkinghub.elsevier.com/retrieve/pii/S092150939700806X.
[28] R. Ritchie, D. Davidson, B. Boyce, J. Campbell, and O. Roder, Fatigue Fract. Eng. Mater. Struct. 22 (1999), p. 621. Available at http://doi.wiley.com/10.1046/j.1460-2695.1999.00194.x.
[29] R.M. Pilliar, Biomaterials 12 (1991), p. 95. Available at http://www.sciencedirect.com/science/article/pii/014296129190185D.
[30] D. Kuroda, M. Niinomi, M. Morinaga, Y. Kato, and T. Yashiro, Mater. Sci. Eng.: A 243 (1998), p. 244. Available at http://linkinghub.elsevier.com/retrieve/pii/S0921509397008083.
[31] H. Choe, S.M. Abkowitz, S. Abkowitz, and D.C. Dunand, Mater. Sci. Eng.: A 396 (2005), p. 99. Available at http://linkinghub.elsevier.com/retrieve/pii/S0921509305000729.
[32] G. Welsch, R.R. Boyer, and E.W. Collings. *Materials Properties Handbook: Titanium Alloys*, ASM International, 1993. Available at http://books.google.com/books?id=x3rToHWOcD8C&pgis=1.
[33] J. Vuorinen and R. Schwarz, J. Compos. Mater. 36 (2002), p. 173. Available at http://jcm.sagepub.com/content/36/2/173.short.
[34] E. Torok and J. Simpson, *Dynamic elastic and damping properties of some practical Ti-base alloys*, Titanium '80 Science and Technology: Proceedings of the 4th International Conference on Titanium, Warrendale, PA, 1980, p. 601.
[35] M. Fukuhara and A. Sanpei, J. Mater. Sci. Lett. 12 (1993), p. 1122. Available at http://link.springer.com/article/10.1007/BF00420541.
[36] M. Landa, P. Sedlák, H. Seiner, L. Heller, L. Bicanová, P. Šittner, and V. Novák, Appl. Phys. A 96 (2009), p. 557. Available at http://link.springer.com/10.1007/s00339-008-5047-4.
[37] J. Nejezchlebová, H. Seiner, M. Ševík, M. Landa, and M. Karlík, NDT & E Int. 69 (2015), p. 40. Available at http://www.sciencedirect.com/science/article/pii/S0963869514001200.
[38] A. Nowick and B. Berry, *Anelastic Relaxation in Crystalline Solids*, Academic Press, New York, 1962.
[39] F. Saigne, L. Dusseau, L. Albert, J. Fesquet, J. Gasiot, J.P. David, R. Ecoffet, R.D. Schrimpf, and K.F. Galloway, J. Appl. Phys. 82 (1997), p. 4102. Available at http://scitation.aip.org/content/aip/journal/jap/82/8/10.1063/1.365721.
[40] Y. Lee and G. Welsch, Mater. Sci. Eng.: A 128 (1990), p. 77. Available at http://www.sciencedirect.com/science/article/pii/092150939090097M.
[41] X. Guan, H. Numakura, M. Koiwa, K. Hasegawa, and C. Ouchi, Mater. Sci. Eng.: A 272 (1999), p. 230. Available at http://www.sciencedirect.com/science/article/pii/S0921509399004645.
[42] R. Wasilewski and G. Kehl, Metallurgia 50 (1954), p. 225.
[43] W. Holman, R. Crawford, and F. Paredes, Trans. Metall. Soc. AIME 233 (1965), p. 1836.
[44] S. Malinov, W. Sha, Z. Guo, C. Tang, and A. Long, Mater. Charact. 48 (2002), p. 279. Available at http://www.sciencedirect.com/science/article/pii/S1044580302002863.
[45] O. Senkov, B. Chakoumakos, J. Jonas, and F. Froes, Mater. Res. Bull. 36 (2001), p. 1431. Available at http://linkinghub.elsevier.com/retrieve/pii/S0025540801006043.
[46] C. Korn and D. Teitel, Phys. Status Solidi A 44 (1977), p. 755. Available at http://onlinelibrary.wiley.com/doi/10.1002/pssa.2210440245/abstract.
[47] H. Asano, Y. Abe, and M. Hirabayashi, Acta Metall. 24 (1976), p. 95. Available at http://www.sciencedirect.com/science/article/pii/0001616076901528.
[48] R. Schaller, G. Fantozzi, and G. Gremaud, *Mechanical Spectroscopy Q-1 2001: With Applications to Materials Science*, Trans Tech Publications Ltd, Clausthal, 2001.
[49] I. Golovin, S. Divinski, J. Čížek, I. Procházka, and F. Stein, Acta Mater. 53 (2005), p. 2581. Available at http://linkinghub.elsevier.com/retrieve/pii/S1359645405001023.

[50] D.H. Niblett, J. Appl. Phys. 32 (1961), p. 895. Available at http://link.aip.org/link/JAPIAU/v32/i5/p895/s1&Agg=doi.
[51] A.S. Nowick and B.S. Berry, *Lognormal distribution function for describing anelastic and other relaxation processes I. theory and numerical computations*. IBM J. Res. Dev. 5 (1961), pp. 297–311.
[52] K. Ushioda, N. Yoshinaga, H. Saitoh, and O. Akisue, *Influences of third elements on snoek peak and the diffusion of C in Ternary Fe-C-M alloys*. Defect Diffus. Forum 95–98 (1993), pp. 375–380.
[53] H. Saitoh, N. Yoshinaga, and K. Ushioda, *Influence of substitutional atoms on the snoek peak of carbon in b.c.c. iron*. Acta Mater. 52 (2004), pp. 1255–1261.
[54] I.S. Golovin, M.S. Blanter, and R. Schaller, *Snoek relaxation in Fe-Cr alloys and interstitial-substitutional interaction*. Phys. Stat. Sol A 160 (1997), pp. 49–60.